

Electronic supplementary information (ESI)

Chiral six-coordinate Dy(III) and Tb(III) complexes of an achiral ligand:
Structure, fluorescence, and magnetism

Mei-Jiao Liu,^a Juan Yuan,^a Yi-Quan Zhang,^{*,b} Hao-Ling Sun,^c Cai-Ming Liu,^d and
Hui-Zhong Kou^{*,a}

^a Department of Chemistry, Tsinghua University, Beijing 100084, P. R. China. Email:
kouhz@mail.tsinghua.edu.cn

^b Jiangsu Key Laboratory for NSLSCS, School of Physical Science and Technology,
Nanjing Normal University, Nanjing 210023, P. R. China. E-mail:
zhangyiquan@njnu.edu.cn

^c Department of Chemistry and Beijing Key Laboratory of Energy Conversion and
Storage Materials, Beijing Normal University, Beijing Normal University, Beijing
100875, P. R. China

^d Beijing National Laboratory for Molecular Sciences, Center for Molecular Science,
Institute of Chemistry, Chinese Academy of Sciences, Beijing 100190, P. R. China

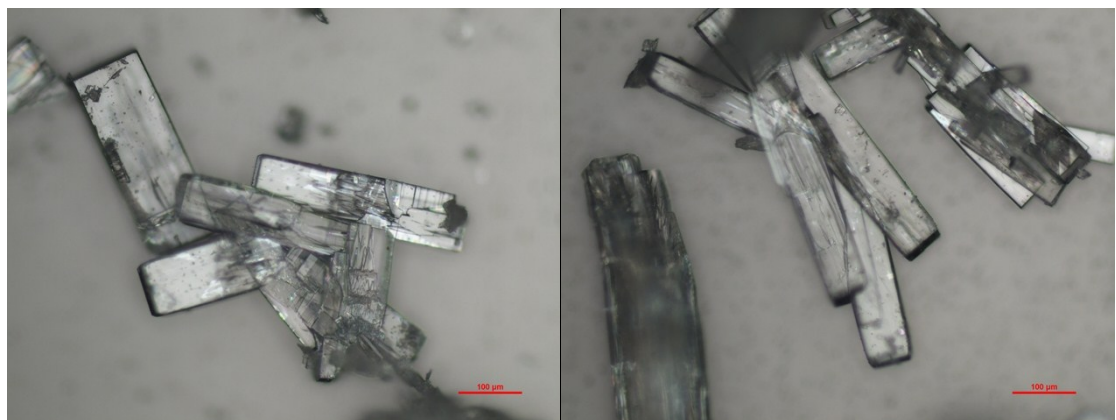


Fig. S1. Crystals under ordinary microscope for complexes **1** (left) and **2** (right).



Fig. S2. Crystals under polarizing microscope from 0° to 85° for complex **1** (five degrees apart).

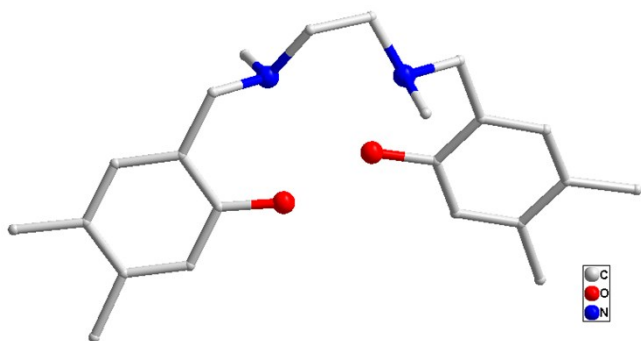


Fig. S3. Crystal structure of the ligand. Hydrogens have been omitted for clarity.

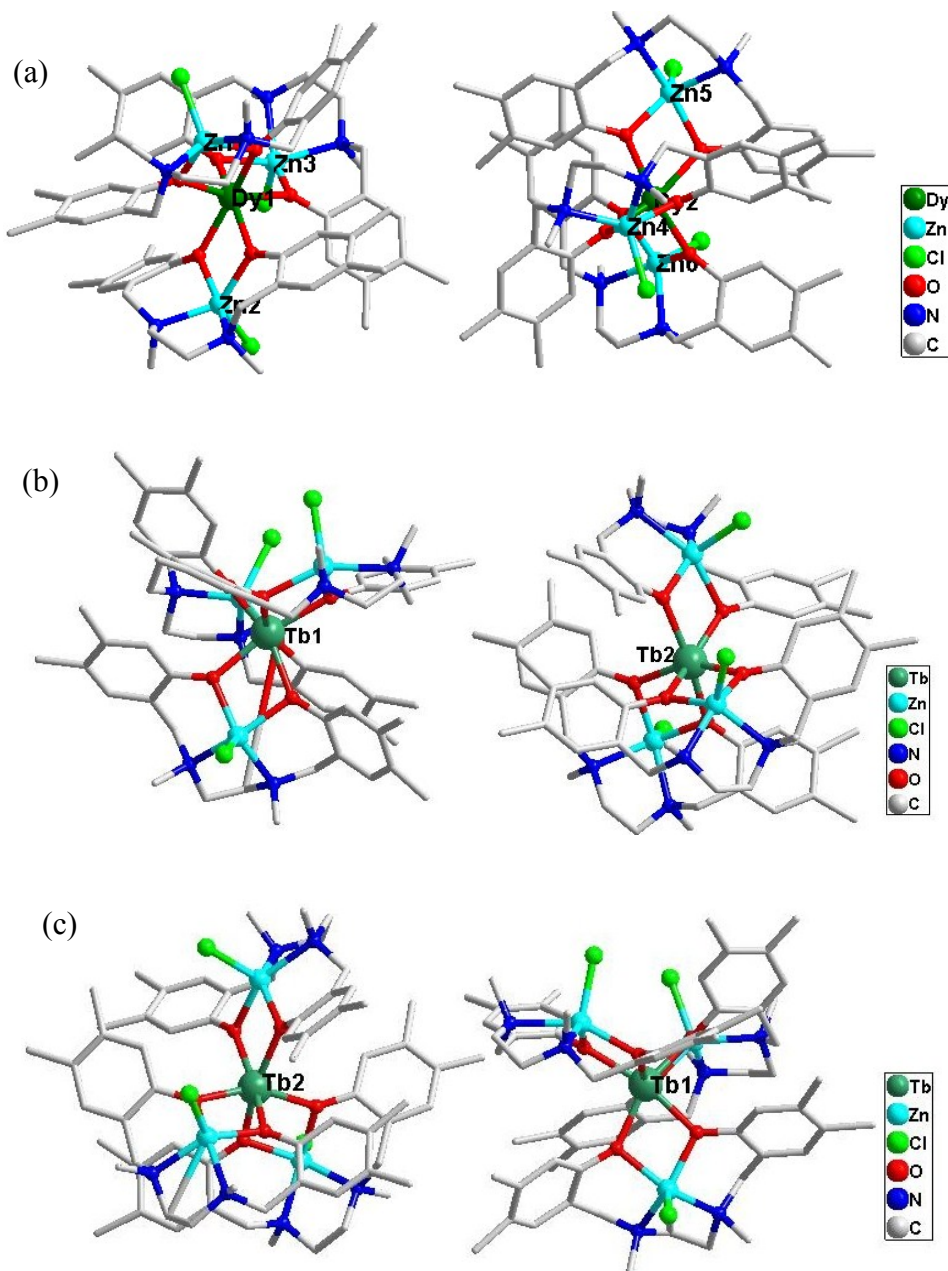


Fig. S4. Main molecular structure of complexes *A*-**1** (a), *A*-**2** and *A*-**2'** (c). Hydrogens and solvents have been omitted for clarity.

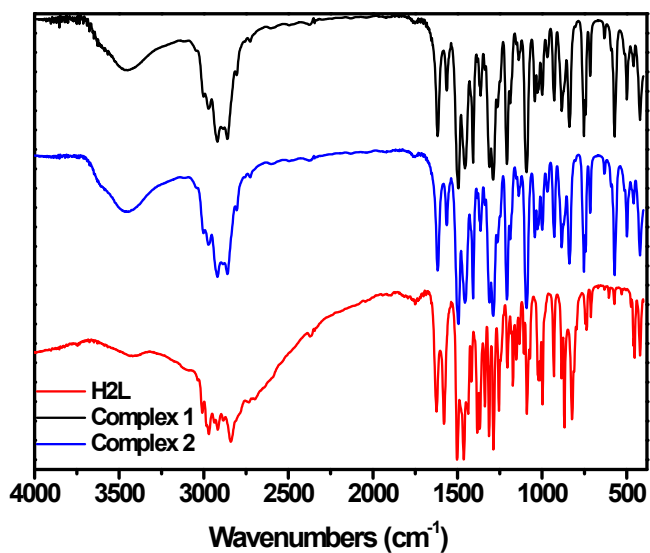


Fig. S5. The IR spectra for the ligand H₂L (red), complex **1** (black) and **2** (blue).

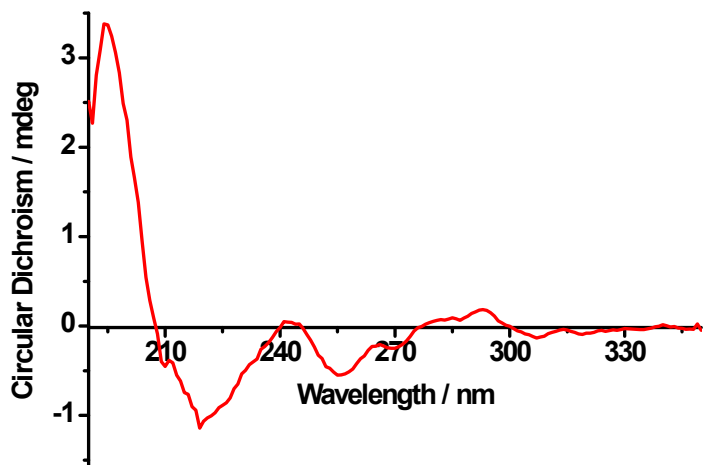


Fig. S6. The solution circular dichroism (CD) spectrum in methanol for complex **1** (100 μmol/L).

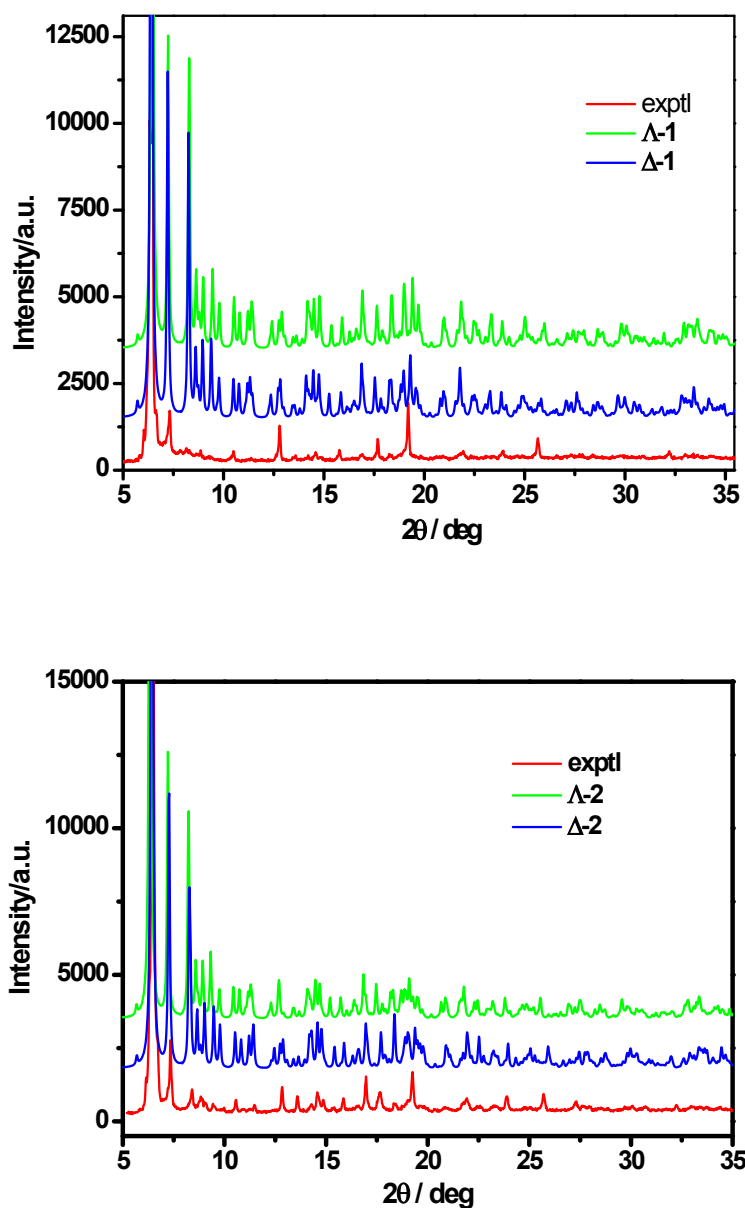


Fig. S7. Powdered X-ray diffraction (XRD) patterns for complexes **1** and **2**.

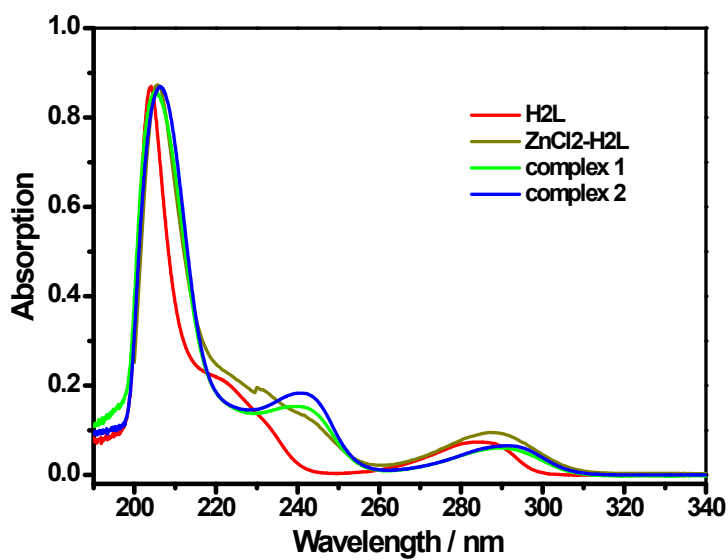


Fig. S8. The solution UV-Vis spectroscopies in methanol for the ligand (red), ZnCl₂-H₂L (brown), complex **1** (green) and complex **2** (blue).

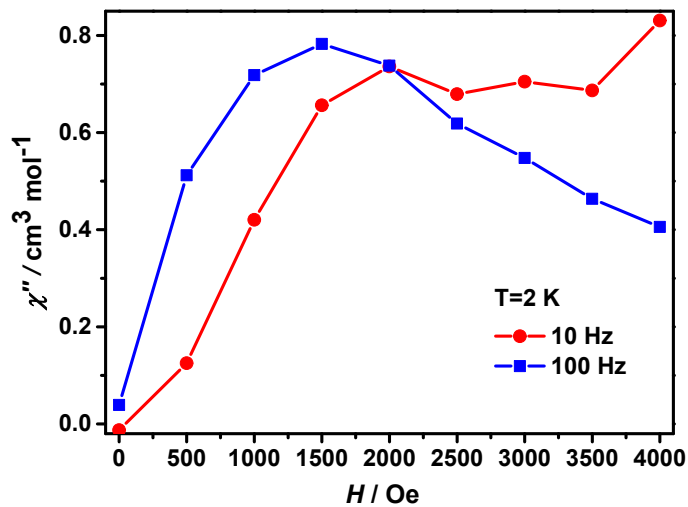


Fig. S9. The out-of-phase component (χ'') vs. external dc field (H) for complex **1** at 2 K with an oscillation of 2.0 Oe and frequencies of 10 Hz and 100 Hz.

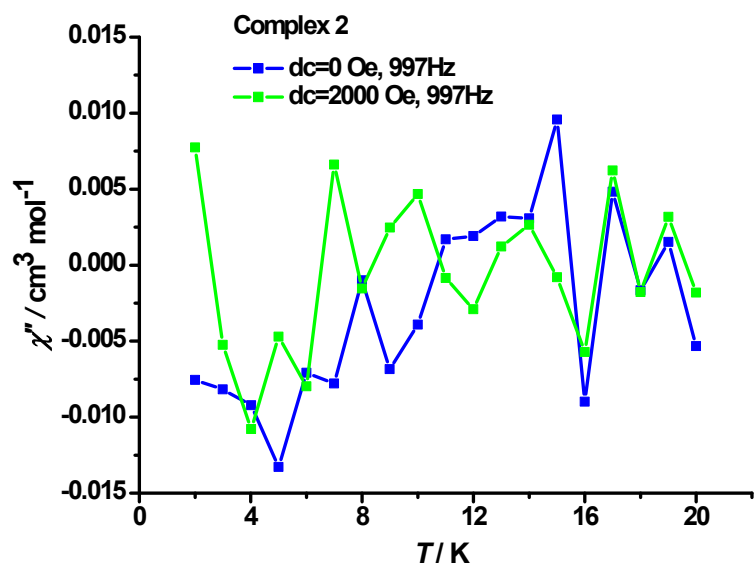


Fig. S10. Temperature dependence of the out-of-phase component (χ'') for complex **2** at 997 Hz.

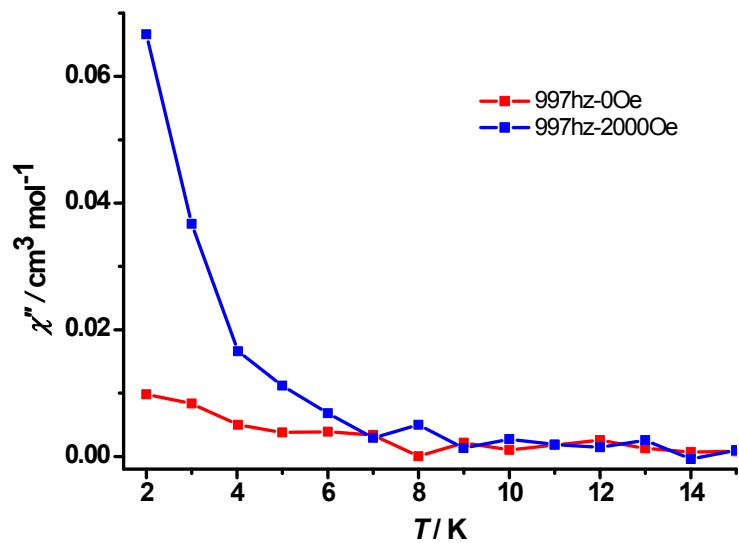


Fig. S11. Temperature dependence of the out-of-phase component (χ'') for diluted sample (Dy_{0.05}Y_{0.95}) of complex **1** at 997 Hz.

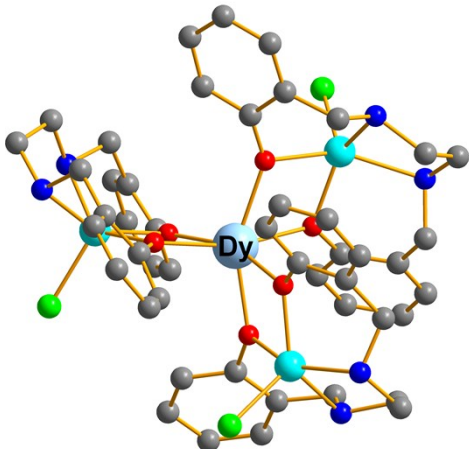


Fig. S12. Calculated complete structure of complex **1**; H atoms are omitted.

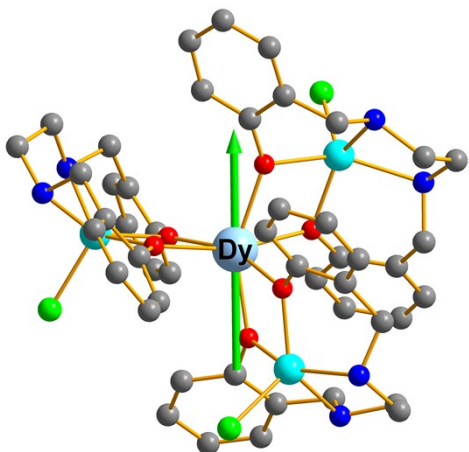


Fig. S13. Orientation of the local main magnetic easy axis of the ground Kramers doublet on Dy^{III} of complex **1**.

Table S1. Calculation results of the lowest Kramers doublets (KDs) of Dy^{III} for complex **1**.

KDs	Complex 1			
	E/cm^{-1}	\mathbf{g}		m_J
1	0.0	g_x	0.089	$\pm 15/2$
		g_y	3.935	
		g_z	15.492	
2	35.2	g_x	0.339	$\pm 3/2$
		g_y	3.069	
		g_z	14.160	
3	71.8	g_x	0.540	$\pm 1/2$
		g_y	1.310	
		g_z	16.026	
4	169.7	g_x	6.386	$\pm 5/2$
		g_y	6.797	
		g_z	7.993	
5	294.6	g_x	0.686	$\pm 11/2$

		g_y	2.376	
		g_z	11.548	
6	318.5	g_x	0.306	$\pm 13/2$
		g_y	1.562	
		g_z	12.414	
7	376.0	g_x	1.182	$\pm 7/2$
		g_y	2.030	
		g_z	16.048	
8	543.9	g_x	0.013	$\pm 9/2$
		g_y	0.035	
		g_z	19.105	

Table S2. In wave functions with definite projection of the total moment $|m_J\rangle$ for the lowest two Kramers doublets (KDs) of the Dy^{III} for complex **1**.

	E/cm^{-1}	wave functions
1	0.0	72% $ \pm 15/2\rangle$ + 5% $ \pm 7/2\rangle$ + 5% $ \pm 3/2\rangle$ + 10% $ \pm 1/2\rangle$
	35.1	17% $ \pm 15/2\rangle$ + 5% $ \pm 13/2\rangle$ + 13% $ \pm 5/2\rangle$ + 24% $ \pm 3/2\rangle$ + 35% $ \pm 1/2\rangle$